Analysis of Radiation From a Line Source in a Grounded Dielectric Slab Covered by a Metal Strip Grating

Yan Kaganovsky, *Student Member, IEEE*, and Reuven Shavit, *Senior Member, IEEE*

***Abstract*—In this paper, we present a study of the radiation from a line source located inside a grounded dielectric slab covered by a metal strip grating. The array scanning method was applied to enable an efficient "unit cell" formulation. The numerical solution was obtained with the use of the spectral method of moments. Both TM and TE cases were solved. The effects of the geometrical parameters on the propagation of guided modes and their excitation are studied.**

***Index Terms*—Array scanning method (ASM), dielectric slab, gratings, Green's function, leaky waves, method of moments (MoM).**

I. Introduction

A METAL STRIP grating over a grounded dielectric slab (MSG-GDS) is a well studied canonical structure with many applications to antennas. Although many studies on the dispersion characteristics of the MSG-GDS can be found in the literature [1]–[5], very little has been reported on the excitation of guided modes by a localized source. It is therefore our aim to investigate the latter. To this end we solve the 2D problem of an MSG-GDS structure excited by a line source. A parametric study on the effect of the geometrical dimensions on the propagation and excitation of guided modes is presented in this paper.

An important part of the source-problem solution is the determination of the modal contributions which in some cases have a dominant effect on the radiating field. Many studies were conducted on the 2D modal waves propagating perpendicular to the strips in the MSG-GDS structure. Most of the studies used approximate methods to obtain their results, such as averaged boundary conditions [1] or rough approximations of the induced currents on the strip grating [2], [3]. These methods can be used only if some restrictions on the structure's geometrical parameters are met, such as electrically small period, narrow slots [3] or thin substrate [2]. A full-wave method which can be used without any restrictions on the geometrical dimensions was presented in [4], [5]. The main focus in these studies was on the propagation of modal waves at an arbitrary angle with respect to the strips and the effect of the propagation angle on the modal characteristics. In [4] the parametric study was conducted only for leaky waves and for a single frequency at a time. In [5] only few results are presented for comparison purposes alone. To the best of our knowledge, a complete parametric study on the effect of the strip's width on the fundamental surface wave (SW) and leaky wave (LW) modes propagating perpendicular to the strips is yet to be reported in the literature. In this paper we report a parametric study on the dispersion characteristics of the MSG-GDS structure for a wide range of frequencies allowing the investigation of an electrically thick substrate. Some previously unreported effects are presented in this paper.

To the best of our knowledge, the only work on the *excitation* of the MSG-GDS structure by a *localized source* was reported in [6] where the "sampling method" was used to calculate the radiation pattern. The sampling method can be applied only to a structure with electrically narrow slots while in this paper we solve without any restrictions. A 3D solution for the TM polarization and a similar structure in which the dielectric slab was replaced by free space and excited by a dipole source was investigated in [7]. In that work reciprocity was exploited in order to replace the original problem with a plane wave scattering problem. Only the effects of dominant LWs were considered in [7] and a parametric study was not presented. The solution in our work was obtained using the "array scanning method" (ASM) [8], [9] which also enables to calculate the SW power, which was previously unpublished for this structure. In addition, we conduct a study on the effects of the geometrical parameters on the radiation pattern and surface wave power. It is noted that a parametric study on the surface wave power for a similar structure in which the substrate's ground plane is absent was presented in [8]. The behavior of the modes in the structure *with* the ground plane present, studied here, is seen to differ from the one studied in [8].

In Section II we present the problem formulation and some theoretical background. In Section III and IV we present the results for the TM and TE cases, respectively. Some conclusions are discussed in Section V.

II. Theory

A. Problem Formulation

The problem under investigation is a metal strip grating over a grounded dielectric slab (GDS) excited by a line source, shown in Fig. 1. In the parametric study which will follow the width of the strip w is varied, while all the other geometrical parameters

Manuscript received January 22, 2008; revised September 07, 2008. Current version published March 04, 2009.

Y. Kaganovsky is with the Department of Electrical Engineering, Tel-Aviv University, Tel-Aviv 69978, Israel (e-mail: yanka@eng.tau.ac.il).

R. Shavit is with the Department of Electrical and Computer Engineering, Ben Gurion University of the Negev, Beer-Sheva 84105, Israel (e-mail: rshavit@ee.bgu.ac.il).

Digital Object Identifier 10.1109/TAP.2008.2009667

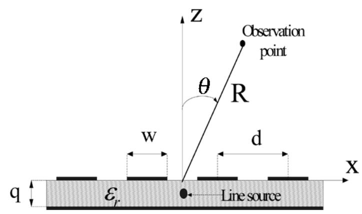

Fig. 1. The structure under investigation consisting of a metal strip grating over a grounded dielectric slab excited by a line source.

of the structure are fixed and their values are given by $\varepsilon_r = 15, q/d = 0.6d = 5.3$ mm. The source is a magnetic line current in the y direction located at $z = -q$ (TM case) which represents a slot excitation, or an electric line current in the y direction located at $z = -q/2$ (TE case).

According to the ASM [8], the solution to the problem in Fig. 1 is obtained by first solving an auxiliary periodic problem in which the line source is duplicated into a phased array of line sources with the same period as the metal grating (d) and a phase difference of $k_x d$. The auxiliary periodic problem is solved using the standard "unit cell" approach. The electric or magnetic fields due to the induced currents on the metal strips in the auxiliary problem can be written as a sum of space harmonics [4]

$$\underline{F}_P^S(x,z;k_x) = \sum_{n=-\infty}^{\infty} \widetilde{\underline{\underline{G}}}(z;k_{xn}) \widetilde{\underline{J}}_S(k_{xn}) e^{-jk_{xn}x} \qquad (1)$$

where $\widetilde{\underline{J}}_S(k_{xn})$ denotes the spectrum of the induced electric or magnetic current on a *single* strip or slot, respectively. $\widetilde{\underline{\underline{G}}}(z;k_{\mathrm{zn}})$ is the spectral dyadic Green's function for a line source in a GDS structure (when electric currents are used) or a line source in a parallel plate (PP) structure (when magnetic currents are used). $k_{xn} = k_x + 2\pi n/d$ is the propagation constant in the x direction of the nth space harmonic. The field $\underline{F}$ (magnetic field in the TM case and the electric field in the TE case) in the original problem of Fig. 1 is obtained from the auxiliary problem solution $\underline{F_P}$ by a spectral integration with respect to the phase variable k_x as explained in [8]. This spectral integral can be expressed as an infinite integral over the 0 th space harmonic of $\underline{F_P}$ denoted here as $\underline{F}_{P0}$ [8].

The periodic auxiliary problem was solved using the periodic spectral method of moments (MoM), choosing standard weighted Chebyshev polynomials as basis and weight functions (Galerkin's method) [4]. The electric field integral equation (EFIE) was used for strip widths which are less than half of the structure's period and the magnetic field integral equation (MFIE) was used for larger strip widths. The MFIE and EFIE formulations can be found in [6] and [8], respectively. The convergence of the numerical solution was tested by increasing the number of the basis functions. A *relative* error below 0.01% was obtained by using 5 basis functions.

B. Asymptotic Evaluation of the Spectral Integral

The transverse propagation constant of the nth space harmonic, given by $k_{\mathrm{zn}} = \pm\sqrt{k_0^2 - k_{xn}^2}$, is a two-valued function. Each of the space harmonics can be chosen to give an exponentially decreasing field in the z direction (proper determination) or an exponentially increasing field in the z direction (improper determination). As a result of this, an infinite set of branch cuts (2 for each space harmonic) must be introduced in order to render the value of the integrand unique. A convenient transformation which maps both Riemann sheets of the 0 th space harmonic (proper and improper) into a single plane is the complex angle transformation which is given by [10]

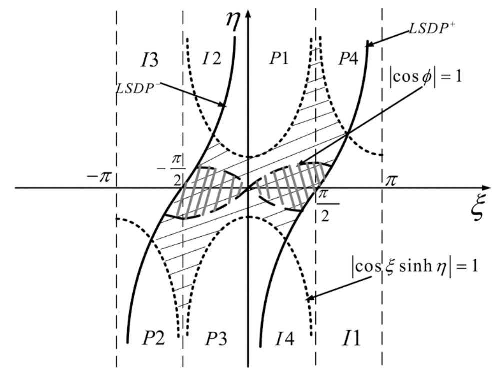

Fig. 2. The complex angle plane. Legend: Ik/Pk— the kth quadrant of the k_x plane on the Improper/Proper Riemann sheet of the 0 th space harmonic, respectively; area with dashed black lines—regions of significant LW pole contributions; area with dashed gray lines—region of oblique radiation.

$$\begin{aligned} &\varphi = \xi + j\eta \\ &k_z = k_0 \cos\varphi, k_x = k_0 \sin\varphi \ = \beta - j\alpha. \end{aligned} \qquad (2)$$

The quadrants of the k_x plane on the proper and improper Riemann sheets of the 0 th space harmonic are mapped into semi-infinite strips shown in Fig. 2 as Pk (proper) and Ik (improper), where the quadrant number is given by $k = 1, 2, 3, 4$. The spectral integral, discussed in Section II.A, can be evaluated asymptotically by deforming the integration contour in the complex angle plane into the steepest descent path (SDP) [10] which intersects the ξ axis at the observation angle θ shown in Fig. 1. The SDPs for $\theta = \pm\pi/2$ are shown in Fig. 2 and are denoted as $LSDP^{\pm}$. In addition to the SDP contribution all branch cuts and poles (not shown in Fig. 2) which are captured between the original integration contour and the SDP must also be taken into account. However, the leading terms for the calculation of the field in the *far-field* zone are the SDP term (also termed the "space wave") which decreases as $O(R^{-1/2})$ away from the structure, and the surface wave (SW) pole terms which account for SWs propagating along the x direction. The directivity calculated from the SDP contribution is given by [8]

$$R_{\mathrm{SDP}}(R,\theta) = \frac{k_0}{2\pi} |F_{P0y}(\theta)|^2 \cos^2\theta \qquad (3)$$

where $F_{P0y}(\theta)$ is the y component of $\underline{F}_{P0}(\theta)$ (the 0 th harmonic of the auxiliary problem solution). The SDP term includes leaky wave (LW) radiation [10] but does not include the end-fire radiation of the SWs.

C. Leaky Wave and Surface Wave Contributions

Despite the fact that the LW *pole* contributions decrease exponentially away from the structure, under some conditions, a LW can be dominant in the *near field* and form the main radiation mechanism by transferring its power to the space wave which carries its power into the far-field zone (see discussion in [11]). By comparing the SDP radiation pattern calculated with (3) to the radiation pattern due to the LW alone, we can determine if the LW is dominant or not. If a good agreement is achieved between the two then the LW is dominant. The criteria for a good agreement chosen here are the direction of maximum radiation, half power beam width and maximum directivity. We calculate the radiation pattern due to a LW alone using a Kirchoff-Huygens integral over the aperture field contributed by a single LW pole, which is given by [12]

$$R_{\mathrm{LW}}(\theta) = \left| \frac{2\sin\phi_p \cos\theta}{\sin^2\theta - \sin^2\phi_p} \right|^2 \quad (4)$$

where $\phi_p = \xi_p + j\eta_p$ is the location of the LW pole which accounts for the radiating space harmonic. If $|\cos\phi_p| < 1$, the radiation pattern in (4) has two maxima at $\theta = \pm\theta_m$ (oblique radiation) given by [12]

$$\cos\theta_m = |\cos\phi_p| = \sqrt{\cosh^2\eta_p - \sin^2\xi_p}. \quad (5)$$

If $|\cos\phi_p| > 1$, there is only one maxima of (4) at $\theta = 0$ (broadside radiation). The boundary of $|\cos\varphi_p| = 1$ is shown as long dashed black lines in Fig. 2.

As discussed in [13], a necessary (but not sufficient) condition for the dominance of a LW in the near field is a relatively small attenuation constant in the x direction, i.e., $\alpha/k_0 = \cos\xi_p \sinh|\eta_p| < 1$ (the boundaries of this region are shown in Fig. 2 as short dashed black lines). In addition, the pole must lie in the visible area (in which the pole can be captured) which boundaries are denoted by $\mathrm{LSDP}^{\pm}$ shown in Fig. 2 as black solid lines. Poles which satisfy both conditions represent possible dominant LWs ("significant LWs"). The possible locations of these poles are shown as the area filled with dashed black lines in Fig. 2. Only poles at these locations need to be considered.

The power carried by the SW modes is calculated separately. The field of the SW modes is calculated from the SW pole contributions by evaluating the residues of the spectral integral at these poles. The technical details can be found in [8]. Since in practice the structure will be finite, the power carried by the SWs will radiate in the form of edge diffraction. In order to evaluate the power lost to this radiation it is customary to divide it by the total radiated power to obtain the SW excitation efficiency.

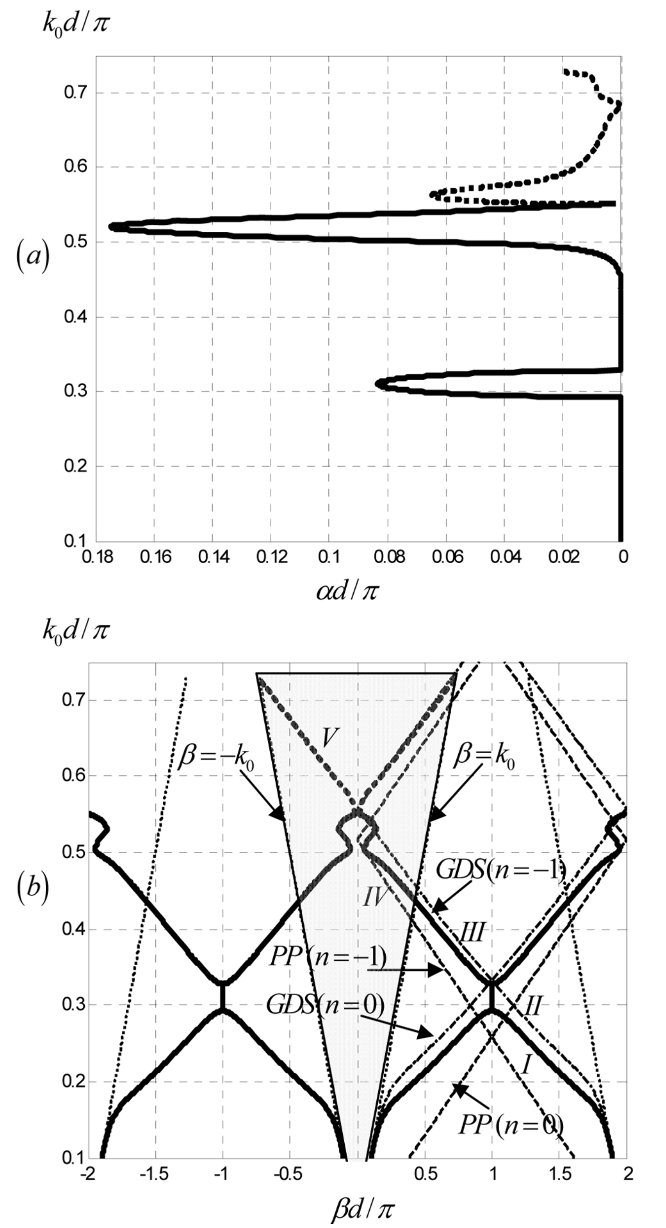

Fig. 3. Dispersion diagram for the fundamental TM modes. (a) attenuation constant versus normalized frequency (b) phase constant versus normalized frequency. Legend: thick solid line—proper mode; thick dotted line—improper mode; dashed line—Floquet harmonics of the PP mode; dashed-dotted line—Floquet harmonics of the GDS mode; dotted lines: $\beta = \pm k_0$. Physical parameters: $\varepsilon_r = 15, q/d = 0.6, w/d = 0.5$.

III. Results for TM Polarization

In the TM case, the electric currents on the strip grating are polarized along the $\widehat{x}$ direction and only the E_x, E_z and H_y components exist.

A. Dispersion Diagram

A full dispersion diagram for the TM case is presented in Fig. 3 for $w/d = 0.5$. This diagram shows the phase (β) and attenuation (α) constants in the x direction of the structure's modes [see (2)] versus normalized frequency. At each frequency there are 2 basic solutions and the rest are merely duplications. For simplicity we discuss the modal solution which starts at the low frequency end at $\beta d/\pi \approx 1.8$. The modal solution can be divided into 5 regions. Region I of the dispersion diagram contains the first SW mode (real solution) which has no cutoff frequency. In region II the structure exhibits a stop-band in which the solutions are evanescent modes and carry negligible power into the far-field zone. After the stop band, a second SW mode exists in region III. At some higher frequency, in region IV, the solution enters the visible region [the gray triangle in Fig. 3(b)] and becomes complex. This solution represents a fast radiating wave $(v_p > c)$ which is termed a LW. All space harmonics of the solutions in regions I-IV are proper.

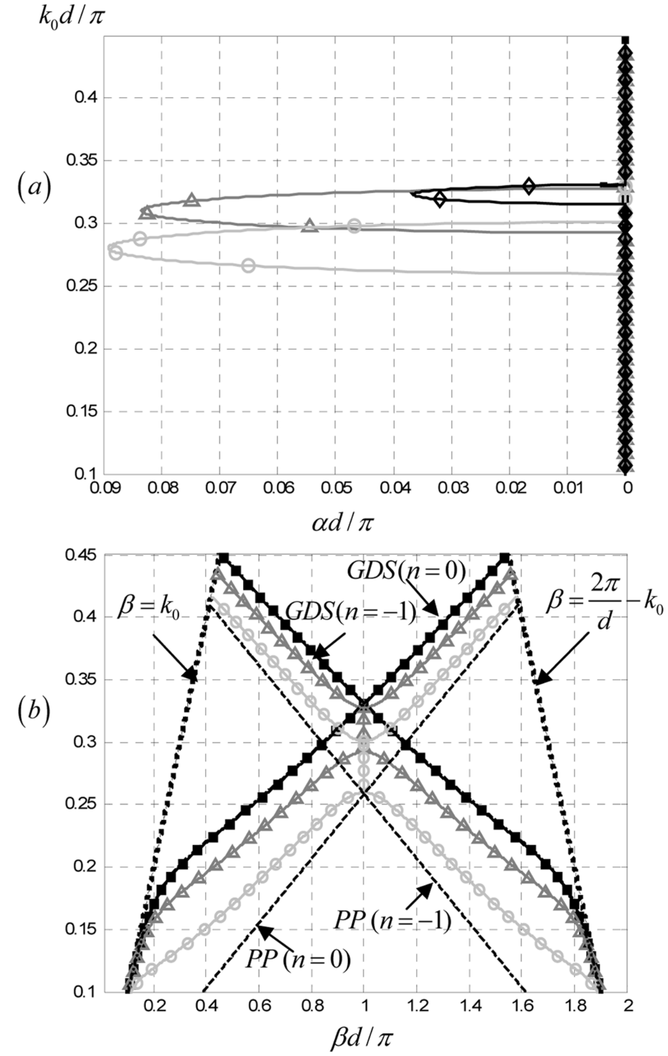

Fig. 4. Dispersion diagram for the fundamental TM surface wave mode in Fig. 3 for different strip widths. (a) Attenuation constant versus normalized frequency (b) phase constant versus normalized frequency. Legend: —○— $w/d = 0.9$; —△— $w/d = 0.5$; —◇— $w/d = 0.3$; —□— $w/d = 0.1$; dashed line—Floquet harmonics of the PP mode; dashed-dotted line—Floquet harmonics of the GDS mode (aligned with $w/d = 0.1$); dotted lines: $\beta = \pm k_0$.

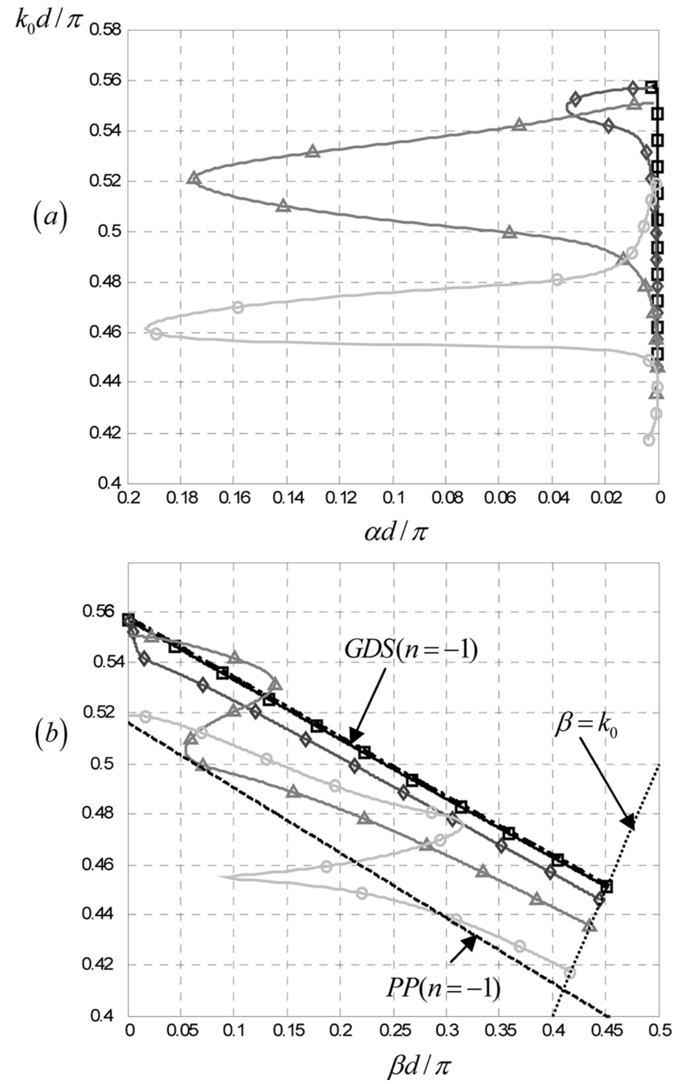

Fig. 5. Dispersion diagram for the fundamental TM proper leaky wave mode in Fig. 3 for different strip widths. (a) Attenuation constant versus normalized frequency (b) phase constant versus normalized frequency. Legend: —○— $w/d = 0.9$; —△— $w/d = 0.5l$; —◇— $w/d = 0.3$; —□— $w/d = 0.1$; dashed line—Floquet harmonics of the PP fundamental mode; dashed-dotted line—Floquet harmonics of the GDS fundamental mode (aligned with $w/d = 0.1$); dotted lines: $\beta = \pm k_0$.

The LW solution in region IV reaches $\beta = 0$ with $\alpha \neq 0$ and continues in the improper Riemann sheet of the 0 th space harmonic (see Fig. 2) where all space harmonics are proper except for the 0 th space harmonic which is improper. This solution is shown in region V of Fig. 3 with dashed lines and is termed the improper LW. In order to understand better the results, we have also included the grounded dielectric slab (GDS) and parallel plate (PP) modes in the dispersion diagram. These modes are obtained by duplicating periodically the ordinary GDS and PP modes. The GDS mode represents a TM mode of a theoretical MSG-GDS structure in which the strip's width goes to zero $(w \rightarrow 0)$. The PP mode serves here only as a boundary for the SW modes.

The SW propagation characteristics for different strip sizes are shown in Fig. 4. One can see that the largest stop band is obtained for the largest strip size (i.e., $w/d = 0.9$). The solution for $w/d = 0.1$ is very close to the GDS mode. This is expected since the current on the strip is perpendicular to the strip and has zero values at the strip's edges so it is negligible for small strip sizes. In the case of $w/d = 0.9$ the solution differs considerably from the PP mode since the electric field is perpendicular to the slots and is not zero at the slot's ends.

The proper LW propagation characteristics for different strip sizes are shown in Fig. 5. It is observed that for strip widths of $w/d > 0.3$, there is a certain frequency range in which the phase constant exhibits an oscillatory behavior accompanied with an increase in the attenuation constant. Fig. 6 shows the LW poles in the complex angle plane and the angle of maximum radiation of the LW $(\theta_{\max})$ versus normalized frequency for various w/d. One can notice a change in the dependency of $\theta_{\max}$ on frequency for $w/d > 0.3$, which corresponds to the strong variations in the propagation constant, observed in Fig. 5. It is seen in Fig. 6(b) that at the low frequency end, the LW beam scans from end-fire towards broadside as the frequency is increased.

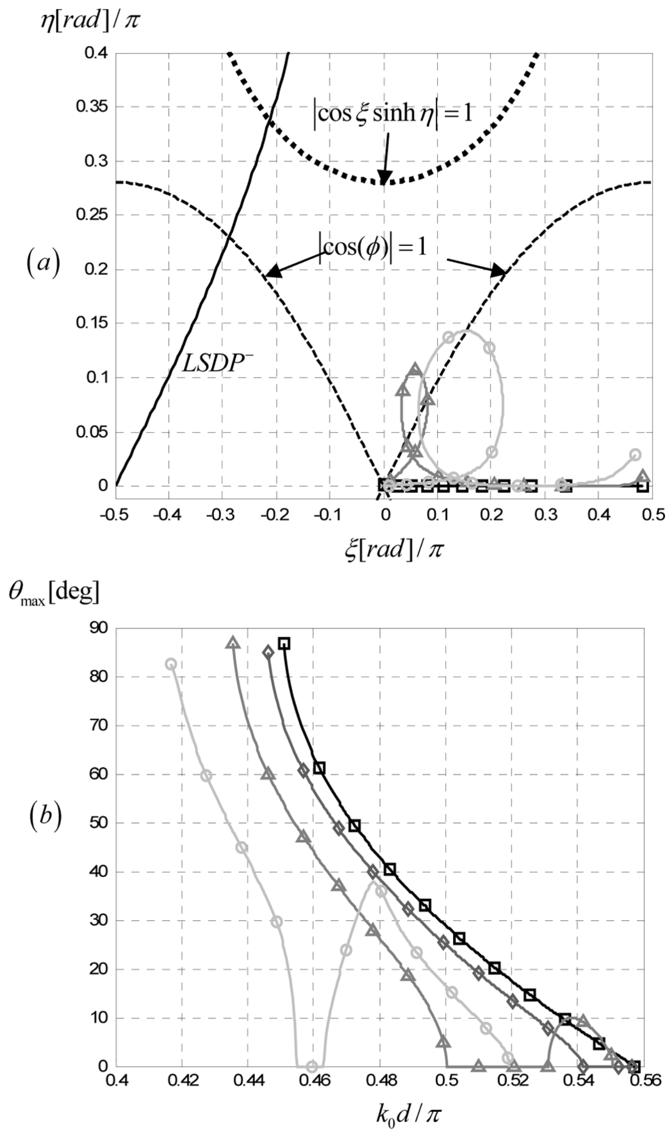

Fig. 6. (a) The loci of the fundamental TM proper leaky wave of Fig. 5 in the complex angle plane versus frequency with varying strip width. (b) Angle of maximum radiation versus normalized frequency. Legend: —○— $w/d = 0.9$; —△— $w/d = 0.5$; —◇— $w/d = 0.3$; —□— $w/d = 0.1$; dashed line—boundaries of the oblique radiation region; solid line—boundary of the visible region; dotted line—boundarries of significant leaky wave solutions.

This frequency band will be termed here "the primary backward scanning band." This band is followed by a frequency band in which the beam is fixed on the broadside direction, which is termed here "the broadside band." In this frequency band the LW poles are located outside the oblique radiation region which boundaries are shown with dashed lines in Fig. 6(a). In the next frequency band the beam scans from broadside towards the end-fire direction as the frequency is raised and is therefore termed here "the forward scanning band." At the high frequency end we identify a frequency band in which the beam scans in a similar manner to the "primary backward band." This band will be termed here "the secondary backward scanning band." It is also observed in Fig. 6(a) that all the LW poles are inside the region of "significant pole contribution" which boundaries appear as solid and dotted black lines.

TABLE I
SUMMARY OF TM PROPER LW DOMINANCE FOR ALL FREQUENCY BANDS

Frequency band	Leaky wave dominance (V= dominant , X= not dominant)
primary backward scanning band	V for all w/d values
broad-side band	X for all w/d values
forward scanning band	X for all w/d values
secondary backward scanning band	V only for small slots i.e. w/d=0.9 or similar values.

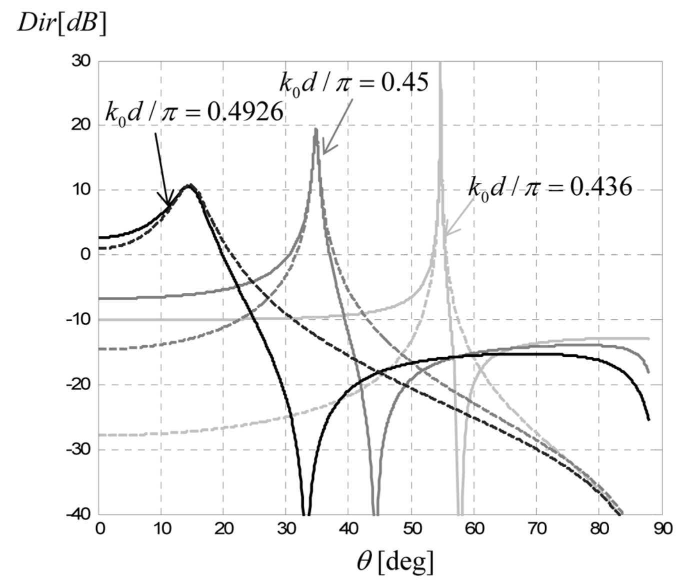

Fig. 7. Directivity for $w/d = 0.5$ in the primary backward scanning band, where a proper dominant leaky wave is supported. Legend: solid line—SDP solution; dashed line- leaky wave.

B. Radiation Pattern

We compare the radiation pattern obtained from (3) with the radiation pattern obtained from the radiating fast harmonics of the LWs, given by (4). We start with the proper LWs. Table I shows a summary of the results that we have obtained for the TM proper LW.

Some examples of radiation patterns in the "primary backward scanning band" with $w/d = 0.5$ are shown in Fig. 7. This band is characterized by a strong variation of the attenuation constant with frequency change for $w/d > 0.3$ (see Fig. 5). Since the attenuation constant controls the beam width [12], this results in a relatively large variation in the beam's width as the frequency is changed. At some frequencies the LW has a very small attenuation constant and this requires a large aperture size in order for the LW to radiate most of its power. This set up can find application whenever the structure's size is relatively large.

An example which shows a poor match between the LW radiation calculation and the SDP calculation is presented in Fig. 8. Fig. 8 shows a radiation pattern in the "forward scanning band" in which the LW is clearly not dominant. This result agrees with the relatively large attenuation constant observed at this

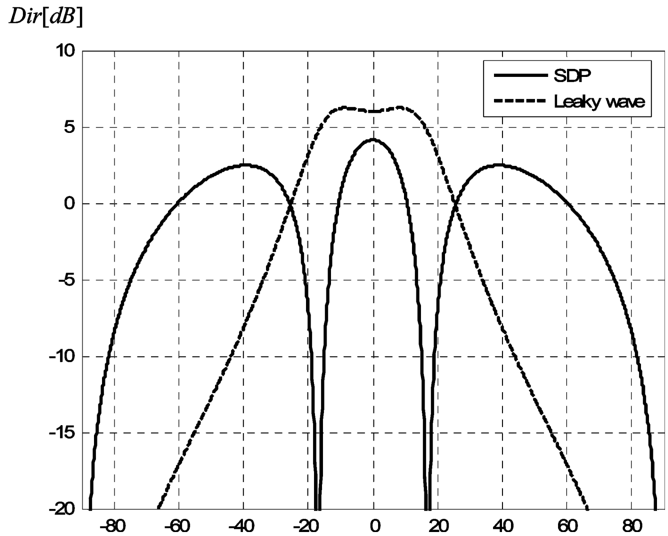

Fig. 8. Directivity for $w/d = 0.5$ in the forward scanning band at $k_0d/\pi = 0.535$, where a proper non dominant leaky wave is supported.

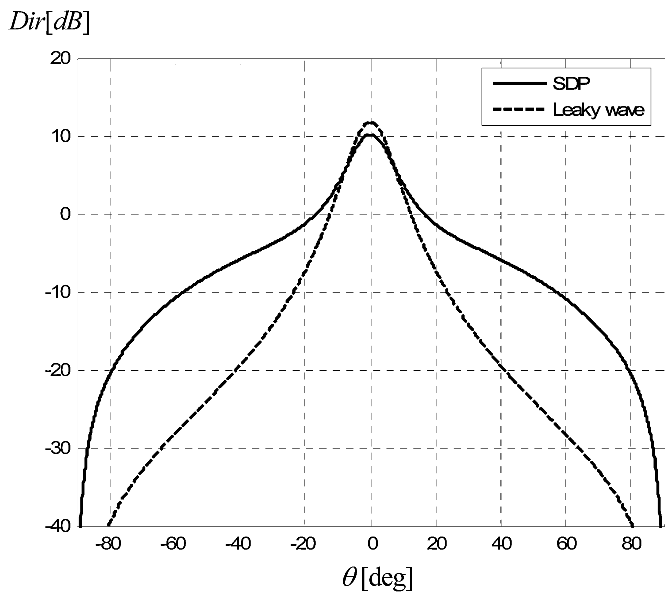

Fig. 9. Directivity for $w/d = 0.5$ in the broad-side band at $k_0d/\pi = 0.56$, where an improper dominant leaky wave is supported.

frequency band (in comparison with other frequency bands) as can be seen in the dispersion diagram of Fig. 3. As discussed in Section II-C, a relatively small attenuation constant is a necessary (although not sufficient) condition for the dominance of the LW.

The TM improper LWs could be investigated only at the lower frequency end since it was later revealed that in addition to the fundamental LW, a higher order LW exists at higher frequencies and it is difficult to separate between the two. The first frequency band of the improper LW is a "broad-side band" whose strong excitation was discovered for all w/d values (the "broad-side band" exists for $w/d \geq 0.3$). An example for the radiation pattern for $w/d = 0.5$ is shown in Fig. 9.

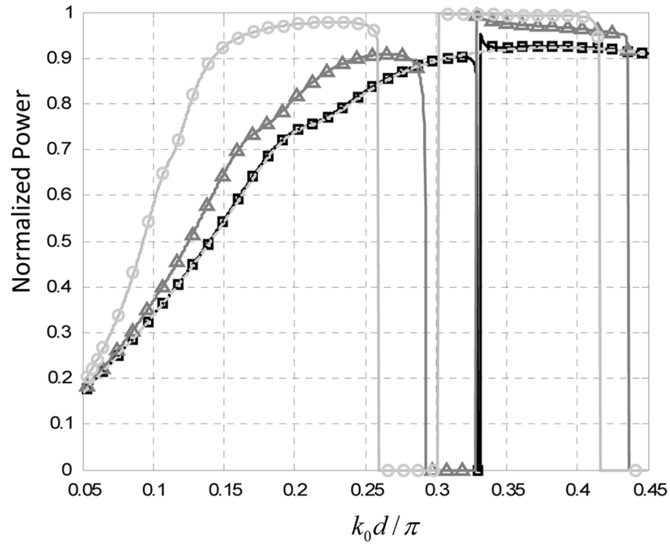

Fig. 10. Surface wave excitation efficiency for different strip sizes. Legend: —○— $w/d = 0.9$; —△— $w/d = 0.5$; —□— $w/d = 0.1$; gray dashed line—GDS without the strip grating (aligned with $w/d = 0.1$) . Physical parameters: as in Fig. 6.

C. Surface Waves Excitation Efficiency

The SW excitation efficiency was calculated using the method outlined in [8]. The results for three different strip widths are shown in Fig. 10. For reference, the efficiency for a GDS structure (without the strip grating) is also plotted in a gray dashed line. The frequency band shown includes both first and second SW modes. It is noted that the calculations are for the far-field region and therefore any evanescent mode carries zero power in this calculation. The zero SW power which can be seen in the middle of the frequency band shown in Fig. 10 occurs at the stop band where the modes are evanescent. It is seen that the largest efficiency is obtained with the smallest slots, as expected. Another conclusion is that for the second SW mode, there is little variation in the efficiency when the strip's size is changed (the efficiency stays above 0.92). It is also seen in Fig. 10 that the MSG-GDS structure with small strips has a SW efficiency which resembles the efficiency of a GDS structure, as expected.

IV. Results for TE Polarization

In the TE case, the electric currents on the strip grating are polarized along the $\hat{y}$ direction and only the H_x, H_z and E_y components exist.

A. Dispersion Diagram

A full dispersion diagram for the TE case is presented in Fig. 11 for $w/d = 0.5$. The modal solutions can be divided into 5 regions similarly to the TM case. The first TE SW mode starts at the normalized frequency $k_0d/\pi = 0.4$. Below this frequency (not shown), the mode continues on the improper Riemann sheet of the 0 th harmonic with a real/complex wave-number (depending on the w/d value), with the prior corresponding to a

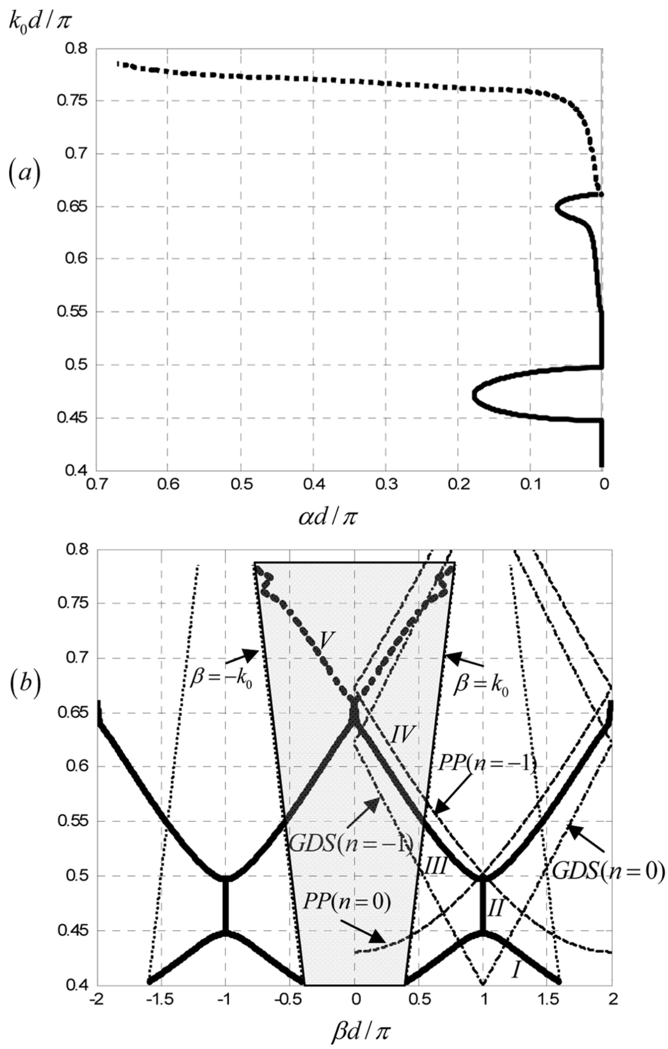

Fig. 11. Dispersion diagram for the fundamental TE modes. (a) Attenuation constant versus normalized frequency (b) phase constant versus normalized frequency. Legend: thick solid line— proper mode; thick dotted line—improper mode; dashed line—Floquet harmonics of the PP mode; dashed-dotted line—Floquet harmonics of the GDS mode; dotted lines: $\beta = \pm k_0$. Physical parameters as in Fig. 3.

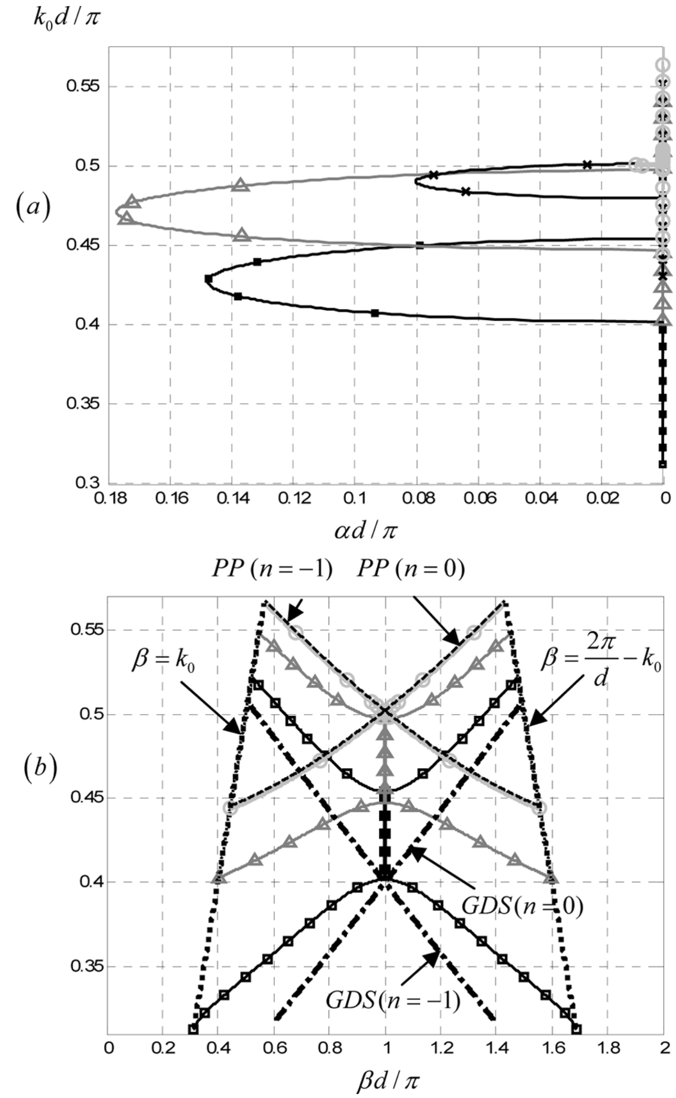

Fig. 12. Dispersion diagram for the fundamental TE surface wave mode in Fig. 11 for different strip widths. (a) Attenuation constant versus normalized frequency (b) phase constant versus normalized frequency. Legend: –○– $w/d = 0.9$; –×– $sw/d = 0.7$; –△– $w/d = 0.5$; –□– $w/d = 0.1$; dashed line—Floquet harmonics of the PP mode; dashed-dotted line—Floquet harmonics of the GDS mode (aligned with $w/d = 0.1$) . Dotted line: $\beta = \pm k_0$.

non physical mode and the latter to a physically meaningful improper LW [14]. A parametric study for this LW mode has been reported in [14] where it was found impractical for most cases.

The SW propagation characteristics for different strip sizes are shown in Fig. 12. One can see that the largest stop band is obtained for the smallest strip size (i.e., $w/d = 0.1$). The solution for $w/d = 0.9$ is very close to the PP solution. This is expected since the electric field in the slot is tangent to the strips, has zero values at the slot's edges and can have little variation along a small slot. The PP mode represents a solution to a theoretical MSG-GDS structure in which the slot's width goes to zero $(w \rightarrow d)$.

The location of the proper and improper LW poles in the complex angle plane and the LW angle of maximum radiation are shown in Fig. 13. It is observed that as opposed to the TM case, there is no oscillatory behavior of the phase constant. In the proper mode regime, there are only 2 frequency bands: a backward scanning band and a small broadside band for $w/d \geq 0.3$. In the improper mode regime there is a forward scanning band, followed by a small backward scanning band (only for $0.1 \leq w/d \leq 0.3$) and a broadside band (in the vicinity of $w/d = 0.5$).

B. Radiation Pattern

Table II summarizes the results obtained for the TE LW.

Some examples for the radiation patterns in the proper "backward scanning band" and improper "forward scanning band" with $w/d = 0.5$ are shown in Figs. 14 (proper) and 15 (improper).

C. Surface Waves Excitation Efficiency

The SW excitation efficiency for three different strip widths is shown in Fig. 16. It is seen that the largest efficiency is obtained with the smallest slot, the same conclusion as in the TM case. As opposed to the TM case, an increase in the slot's width beyond

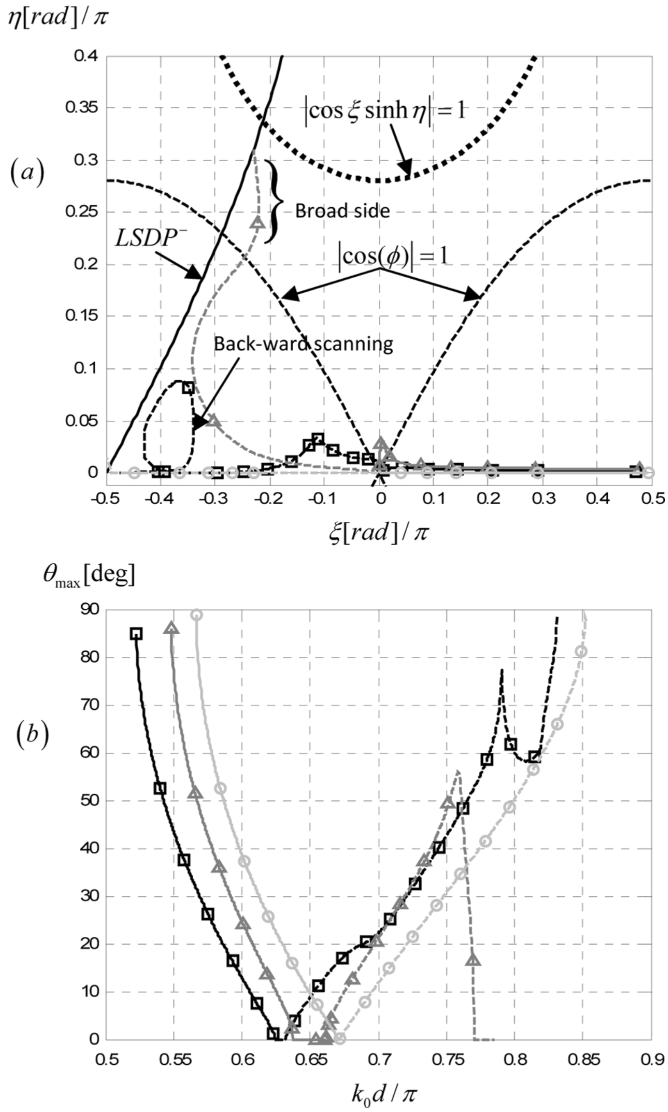

Fig. 13. (a) The loci of the fundamental TE proper and improper leaky waves of Fig. 11 in the complex angle plane versus frequency with varying strip width. (b) angle of maximum radiation versus normalized frequency. Legend: –○– $w/d = 0.9$; –△– $w/d = 0.5$; –□– $w/d = 0.1$; solid line with marker—proper leaky wave; dashed line with marker—improper leaky wave; dashed line—boundaries of the oblique radiation region; solid line—boundary of the visible region; dotted line—boundary of significant leaky wave solutions.

TABLE II
SUMMARY OF TE LW DOMINANCE FOR ALL FREQUENCY BANDS

Frequency band	Leaky wave dominance (V= dominant , X= not dominant)
proper backward scanning band	V for all w/d values
proper broad-side band	V for all w/d values
improper forward scanning band	V for all w/d values
improper backward scanning band	X for all w/d values
improper broad-side band	X for all w/d values

$w/d = 0.5$ decreases considerably the efficiency of the second SW mode. It should be noted that for $w/d = 0.9$ we have a PP mode [see Fig. 12(b)] so most of the power is contained inside the dielectric slab and the SW efficiency is very close to 1, as seen in Fig. 16.

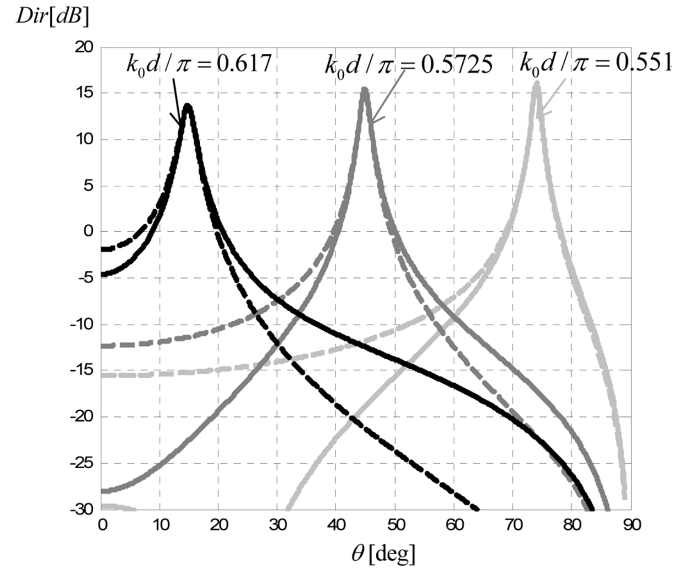

Fig. 14. Directivity for $w/d = 0.5$ in the backward scanning band where a proper dominant leaky wave is supported. Legend: solid line—SDP solution; dashed line- leaky wave.

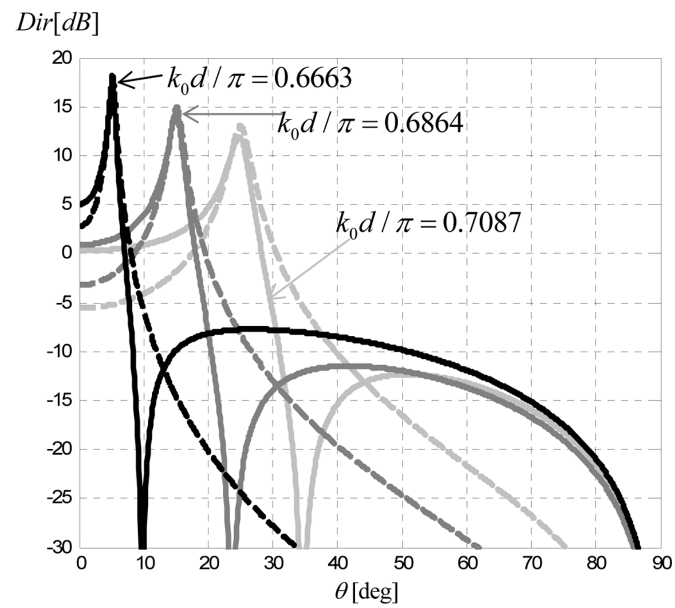

Fig. 15. Directivity for $w/d = 0.5$ in the forward scanning band where an improper dominant leaky wave is supported. Legend: solid line—SDP solution; dashed line- leaky wave.

V. CONCLUSION

The problem of line source excitation of an MSG-GDS structure was solved using the ASM and the periodic MoM. Both EFIE and MFIE formulations were used in order to obtain an efficient solution for all possible values of the structural parameter (the strip width in the metal grating). The main focus in this work was on the effect of the structural parameters on the excitation of modes and their radiation characteristics.

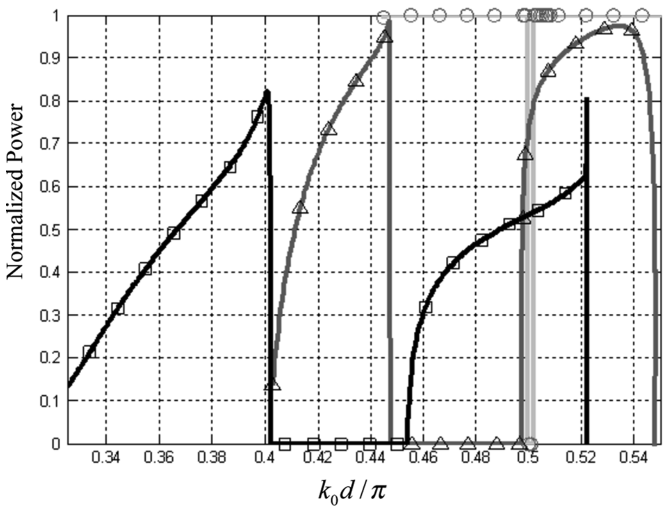

Fig. 16. Surface wave excitation efficiency for different strip sizes. Legend: $-\bigcirc- w/d = 0.9$; $-\triangle- w/d = 0.5$; $-\square- w/d = 0.1$; Physical parameters: as in Fig. 3.

A parametric study was presented in which the effect of the strip width on the propagation of SWs and LWs was demonstrated. The stop band was investigated and it was found that the largest stop band is obtained with small slots in the TM case and with small strips in the TE case. It was also found that in some cases the fundamental TM proper LW exhibits a strong variation of its propagation characteristics which introduces a variety of different radiation characteristics. The TE LW was investigated in both proper and improper regimes.

The excitation of LWs was investigated by comparing the LW radiation pattern with the total radiation pattern due to the line source excitation. It was found that the TM proper LW is dominant only in the backward scanning bands and that all bands in the transition area, characterized by a strong variation of the propagation constant with frequency change, cannot be used for LW antenna applications. It was shown that the TM improper LW can be used for broad-side radiation. The proper TE LW was found to be dominant in all frequency bands and the improper TE LW was shown to be dominant only in the forward scanning band.

The SW excitation efficiency was calculated by comparing the SW power with the total radiated power. Both TM and TE SWs showed the strongest excitation for small slots. The second TM SW showed very little change in the excitation efficiency as the slot's width was increased, whereas, in the TE case the second mode showed a considerable decrease in efficiency.

REFERENCES

[1] F. H. Bellamine and E. F. Kuester, "Guided waves along a metal grating on the surface of a grounded dielectric slab," *IEEE Trans. Mocrow. Theory Tech.*, vol. 42, no. 7, pp. 1190–1197, Jul. 1994.

[2] J. Jacobsen, "Analytical, numerical, and experimental investigation of guided waves on a periodically strip-loaded dielectric slab," *IEEE Trans. Antennas Propag.*, vol. AP-18, no. 3, pp. 379–388, May 1970.

[3] R. A. Sigelman, "Surface waves on a grounded dielectric slab covered by a periodically slotted conducting plane," *IEEE Trans. Antennas Propag.*, vol. AP-15, pp. 672–676, Sep. 1967.

[4] P. Baccarelli, P. Burghignoli, C. Di Nallo, F. Frezza, A. Galli, P. Lampariello, and G. Ruggieri, "Full wave analysis of printed leaky wave phased arrays," *Int. J. RF Microw. Comput. Aided Eng.*, vol. 12, pp. 272–287, May./Jun. 2002.

[5] P. Baccarelli, P. Burghignoli, C. Di Nallo, F. Frezza, A. Galli, P. Lampariello, G. Lovat, and S. Paulotto, "Modal properties of surface and leaky waves propagation at arbitrary angles along a metal strip grating on a grounded slab," *IEEE Trans. Antennas Propag.*, vol. 53, no. 1, pp. 36–46, Jan. 2005.

[6] R. A. Sigelman and A. Ishimaru, "Radiation from periodic structures excited by an aperiodic source," *IEEE Trans. Antennas Propag.*, vol. AP-13, pp. 354–364, May 1965.

[7] G. Lovat, P. Burghignoli, F. Capolino, D. R. Jackson, and D. R. Wilton, "High-gain omnidirectional radiation patterns from a metal strip grating leaky-wave antenna," in *IEEE Antennas Propag. Int. Symp.*, Honolulu, HI, Jun. 10-15, 2007, pp. .5797–5800.

[8] H. D. Yang and D. R. Jackson, "Theory of line-source radiation from a metal-strip grating dielectric-slab structure," *IEEE Trans. Antennas Propag.*, vol. 48, no. 4, pp. 556–564, Apr. 2000.

[9] V. Galindo, "A generalized approach to a solution of aperiodic arrays and modulated surfaces," *IEEE Trans. Antennas and Propag.*, vol. AP-16, no. 4, Jul. 1968.

[10] L. B. Felsen and N. Marcuvitz, *Radiation and Scattering of Waves*, ser. IEEE Press Series on Electromagnetic Waves, 2nd ed. Englewood Cliffs, NJ: Prentice Hall, 1994.

[11] T. Tamir and A. A. Oliner, "Guided complex waves—Part 1. fields at an interface," in *Proc. Inst. Elect. Eng.*, Feb. 1963, vol. 110, no. 2, pp. 310–324.

[12] R. E Collin and F. J. Zucker, *Antenna Theory—Part2*. New York: McGraw-Hill, 1969, ch. 20.

[13] T. Tamir and A. A. Oliner, "Guided complex Waves—Part 2. relation to radiation pattern," in *Proc. Inst. Elect. Eng.*, Feb. 1963, vol. 110, no. 2, pp. 325–334.

[14] P. Burghignoli, P. Baccarelli, F. Frezza, A. Galli, P. Lampariello, and A. A Onliner, "Low- frequency dispersion features of a new complex mode for a periodic strip grating on a grounded dielectric slab," *IEEE Trans Microw. Theory Tech.*, vol. 49, no. 12, Dec. 2001.

Yan Kaganovsky (S'07) was born in Tel-Aviv, Israel, in February 1977. He received the B.Sc. and the M.Sc. (*summa cum laude*) degrees in electrical engineering, both from Ben Gurion University, Israel, in 2004 and 2007, respectively. He is currently working toward the Ph.D. degree at Tel Aviv University.

His main fields of interest are wave propagation in periodic structures and inhomogeneous media, and analytical methods for time domain wave phenomena.

Reuven Shavit (M'82–SM'90) was born in Rumania on November 14, 1949. He received the B.Sc. and M.Sc. degrees in electrical engineering from the Technion-Israel Institute of Technology, Haifa, Israel, in 1971 and 1977, respectively, and the Ph.D. degree in electrical engineering from the University of California, Los Angeles, in 1982.

From 1971 to 1993, he worked as a Staff Engineer and Antenna Group Leader in the Electronic Research Laboratories, Israeli Ministry of Defense, Tel Aviv, where he was involved in the design of reflector, microstrip, and slot antenna arrays. He was also a part-time lecturer at Tel Aviv University, teaching various antenna and electromagnetic courses. From 1988 to 1990 he was associated with ESSCO, Concord, MA, as a Principal Engineer involved in scattering analysis and tuning techniques of high performance ground based radomes. Currently, he is with Ben-Gurion University of the Negev, as an Associate Professor doing research in microwave components and antennas. His present research interest is in the areas of smart antennas, tuning techniques for radomes and numerical methods for design microstrip, slot and reflector antennas.